Role of Microbes in the Smectite-to-Illite Reaction

Jinwook Kim,[1]*† Hailiang Dong,[2]† Jennifer Seabaugh,[2]
Steven W. Newell,[1] Dennis D. Eberl[3]

Temperature, pressure, and time have been thought to control the smectite-to-illite (S-I) reaction, an important diagenetic process used for petroleum exploration. We demonstrated that microorganisms can promote the S-I reaction by dissolving smectite through reduction of structural Fe(III) at room temperature and 1 atmosphere within 14 days. This reaction typically requires conditions of 300° to 350°C, 100 megapascals, and 4 to 5 months in the absence of microbial activity. These results challenge the conventional concept of the S-I reaction and of reaction kinetic models.

The smectite-to-illite (S-I) reaction is closely related to hydrocarbon maturation (*1*), geopressuring of shale (*2*), the formation of growth faults (*3*), and changes in pore water chemistry (*4*). The S-I reaction occurs approximately concomitantly with the maturation of petroleum during sediment diagenesis. The degree of S-I reaction is frequently used as a geothermometer to allow reconstructions of the thermal and tectonic history of sedimentary basins (*5*). Numerous studies have emphasized temperature, pressure, and time as geological variables in either solid-state or dissolution-precipitation S-I reaction mechanisms (*6*, *7*).

Here we present evidence for the neoformation of illite as a result of microbial dissolution of smectite through reduction of Fe(III) in the smectite structure, which suggests that microbes play an important role in the S-I reaction. *Shewanella oneidensis* strain MR-1, a dissimilatory metal-reducing bacterium, was incubated with Fe-rich smectite [nontronite, $(Ca, Na, K)_{1.05}[Si_{6.98}Al_{1.02}][Al_{0.29}Fe_{3.68}Mg_{0.04}]O_{20}(OH)_4$] obtained from the Clay Minerals Society (sample NAu-1) (*8*) as a sole electron acceptor and with formate as an electron donor for 14 days under anaerobic conditions (*9*, *10*). The bioproduced Fe(II) concentration, as measured by Ferrozine assay (*11*), increased with time (Fig. 1), and the extent of reduction reached 43% in 14 days. MR-1 cells were viable by the end of incubation. Controls consisted of solutions that received cells killed by microwave radiation in place of live log-phase cells, and they did not show any reduction (Fig. 1).

Transmission electron microscope (TEM) lattice fringe images of the nonreduced control samples showed typical 1.3-nm spacings, suggesting that smectite was the only clay phase present, and there was no evidence of any dissolution. However, we observed two types of clay phases in the microbially Fe(III)-reduced sample at the end of the 14-day incubation (Fig. 2): (i) layers of 1.3-nm spacing with wavy and variable fringes and layer terminations, which are typical of smec-

[1]Naval Research Laboratory, Seafloor Sciences Branch, Stennis Space Center, MS 39529, USA. [2]Department of Geology, Miami University, Oxford, OH 45056, USA. [3]U.S. Geological Survey, Boulder, CO 80303, USA.

*To whom correspondence should be addressed. E-mail: jkim@nrlssc.navy.mil
†These authors contributed equally to this work.

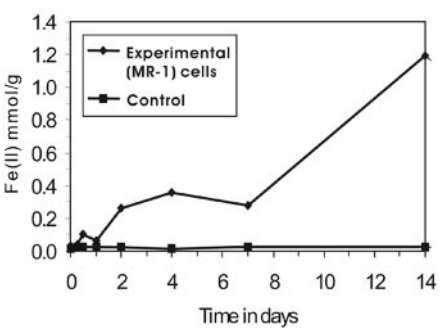

Fig. 1. Change of HCl-extractable Fe(II) with time in the Fe-rich smectite control and in the experimental (MR-1) tubes. The measured HCl-extractable Fe(II) concentration (mM) was normalized to milligrams of smectite in each tube and reported as mmol/g. The extent of reduction by the end of incubation reached 43%, based on measured Fe(III) concentration and the amount of smectite used in the tubes. The vertical errors are typically <10%.

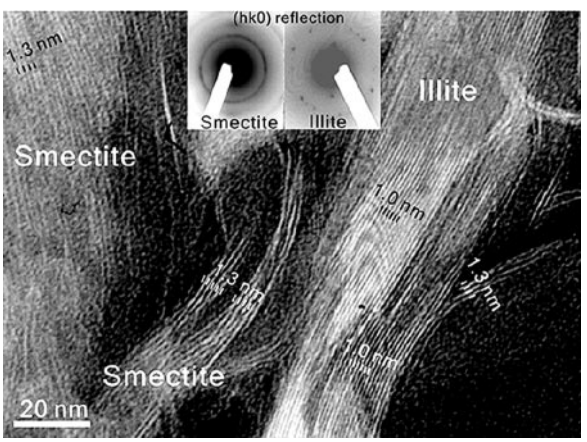

Fig. 2. TEM micrograph of the L.R. White resin–embedded bioreduced smectite sample. Two phases of clay minerals were observed: An approximately 40-nm-thick packet of 1.0-nm illite layers occurred in the smectite matrix of 1.3-nm layers. The inset SAED patterns show the structural difference between these two phases in (*hk*0) reflections, in ring patterns (turbostratic typical of the smectite structure), and in discrete Bragg reflections (typical of the illite structure).

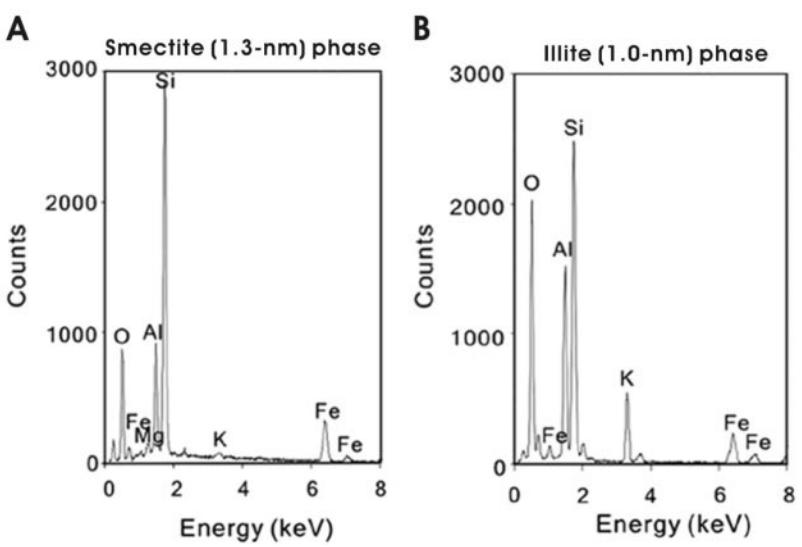

Fig. 3. Energy-dispersive x-ray spectroscopy spectra of the two phases observed in the bioreduced smectite sample. (**A**) The smectite (1.3-nm) phase having low Al/Si (0.19) and low K values. (**B**) The illite (1.0-nm) phase having high Al/Si (0.61) and high K values.

tite; (ii) layers of 1.0-nm spacing with continuous and defect-free fringes, which are typical of illite. These two phases were observed in an approximately 40-nm-thick packet of 1.0-nm layers in the smectite matrix, indicating that the previously occupied 1.3-nm smectite layers were neoformed to a 1.0-nm illite phase as a result of microbial activity.

Quantitative energy-dispersive x-ray spectroscopy analyses (Fig. 3) on the 1.3-nm phase showed a typical composition for smectite, with relatively abundant Fe (Fig. 3A), whereas the 1.0-nm phase had Al/Si ratios (0.61 in average) similar to those of illite [0.60 (*12*) and 0.58 (*13*)] (Fig. 3B). There was a significant increase in K and decrease in Si in the illite as compared with the smectite. Glauconite also had a 1.0-nm spacing; however, its Al/Si ratio had much lower values [0.163 (*14*) and 0.196 (*15*)].

The air-dried, bioreduced smectite sample had an x-ray diffraction (XRD) peak with a 2θ value at 8.82° (using Cu K-α radiation) that corresponds to a 1.0-nm d-spacing (Fig. 4A). The sample was then treated with polyvinylpyrrolidone (PVP). PVP is preferentially sorbed on silicate surfaces, causing x-ray incoherency for smectite particles, leading to the disappearance of smectite x-ray reflections (*16*). Thus, the intensification of the 1.0-nm peak after PVP treatment suggests the presence of illite. The crystal size distribution (CSD) of the neoformed illite by XRD (*17*) followed an asymptotic shape that was different from those found for smectite in the nonreduced control and in the bioreduced sample (Fig. 4B). The mean crystal size of the neoformed illite was 11.2 nm with β^2 = 0.75 and α = 2.06 nm, where β^2 is the variance of the natural logarithms of the crystal thicknesses, and α is the mean of the natural logarithms of the crystal thicknesses. The mean crystal thicknesses for air-dried samples of smectite in the control and the bioreduced sample were similar: 5.1 nm with β^2 = 0.19 and α = 1.53 nm, and 5.3 nm with β^2 = 0.16 and α = 1.51 nm, respectively, indicating that the CSD of the neoformed illite phase is different from that of smectite. The theoretical crystal growth path (*18*) through α and β^2 space [curve 4 in figure 12 of (*18*)] suggests that the newly formed illite in the bioreduced sample grows by a continuous nucleation and growth mechanism, implying the reductive dissolution of smectite and simultaneous precipitation of illite.

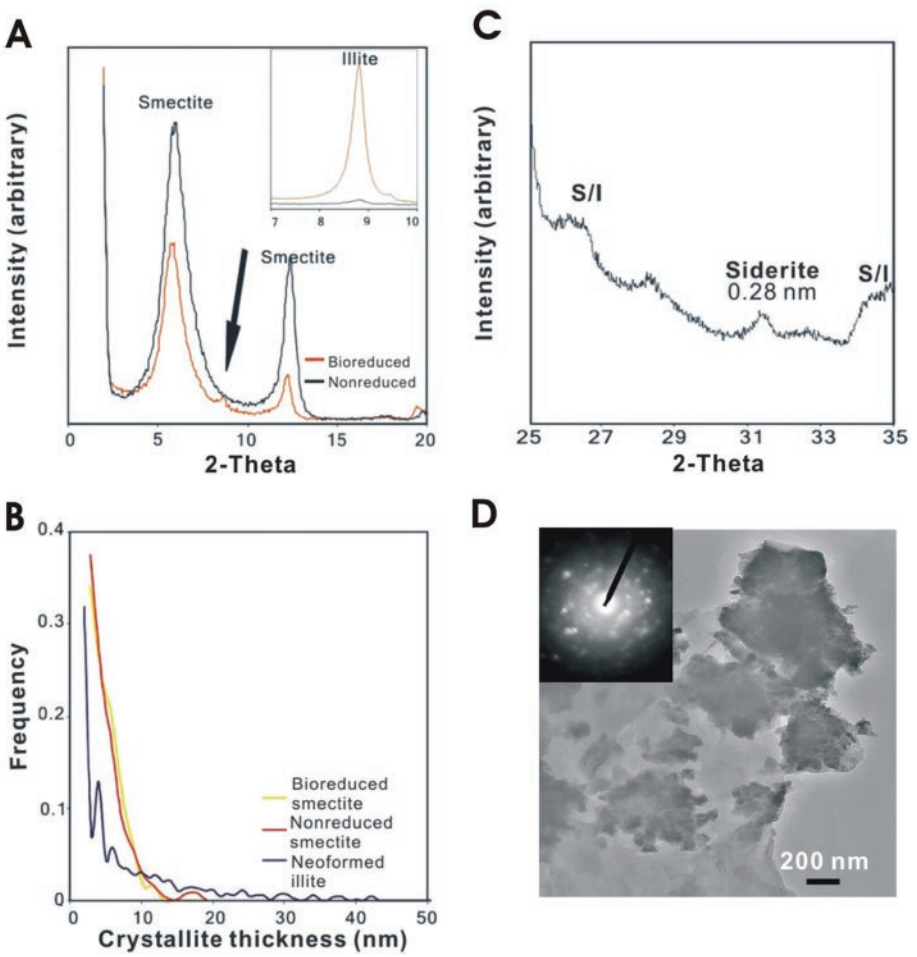

Fig. 4. Detection of the neoformed illite phase by XRD and TEM. (**A**) XRD profiles for the air-dried, bioreduced smectite sample (red) and the nonreduced control (black). Both the smectite and the illite phase were detected with 2θ at 5.92° and 8.82°, respectively, in the bioreduced smectite sample, whereas only the smectite peak at the same 2θ angle appears in the nonreduced control. The illite peak intensified by the PVP treatment (inset) is evident in the bioreduced smectite sample. (**B**) CSD of the neoformed illite phase (blue) in the bioreduced smectite sample showing a different asymptotic shape as compared with that of smectite (red) in the nonreduced control and the smectite phase (yellow) in the bioreduced sample. (**C**) Detection of Fe-rich mineral precipitates by XRD. The peak with 2θ at 31.6° is identified as siderite (Fe-carbonate), a byproduct of a reductive dissolution of smectite. The broad S-I peak is also shown. (**D**) Detection of Fe-rich mineral precipitates by TEM and SAED pattern (inset). The aggregates shown in the TEM micrograph are identified as a mixture of siderite and vivianite grains by SAED pattern. d-spacings of 0.68, 0.27, and 0.29 nm, typical of siderite, and of 0.28, 0.36, and 0.19 nm, typical of vivianite, were measured.

Excess Fe resulting from the reductive dissolution of Fe-rich smectite can cause precipitation of Fe-rich minerals as byproducts, because illite contains less Fe than does smectite (Fig. 3). Approximately 10% of the total bioproduced Fe(II), as measured by the Ferrozine method (*11*), was detected in aqueous solution, indicating that most biogenic Fe(II) was in solids. Indeed, siderite ($FeCO_3$) was detected in the bioreduced smectite sample (Fig. 4, C and D) but not in the control. Abundant bicarbonate was available in the M1 medium. The peak with a 2θ value at 31.6° corresponding to 0.28-nm spacing (Fig. 4C) is the most intense peak of siderite (x-ray powder diffraction database JCPDS card 29-696). Because the M1 medium also contained phosphate, vivianite formation was a possibility. Vivianite was not present in the XRD pattern but was detected by selected-area electron diffraction (SAED) (Fig. 4D), suggesting its relatively low abundance.

Thus, microbes can promote the S-I reaction via the dissolution of smectite. Smectite dissolution was made possible by reduction of structural Fe(III) in the smectite structure. Considering the decrease of the positive charge in the octahedral sheet as a result of reduction of Fe(III), it is not surprising to observe K uptake into the interlayers to balance the charge and thus to produce illite. Abundant K was available in the medium. Our XRD and TEM data collectively show that bacteria promoted the S-I reaction and that the reaction mechanism was via the dissolution of reactant smectite and the neoformation of product illite.

Other studies support our conclusion that reduction of Fe(III) to Fe(II) can drive the S-I reaction. For example, Cretaceous bentonites show an increasing percentage of illite layers in mixed-layered illite-smectite (I-S) with overall increasing Fe^{2+}/Fe^{3+} (*19*). A small

amount of a mica-like (same as illite-like) phase (with 1.0-nm spacing) was also observed (*20*) when Fe-rich smectite was chemically reduced by dithionite. However, dithionite is not likely to occur in abundance or to play a substantial role in iron reduction in natural soil environments. In this study, we have shown that bacteria can play an important role in driving the S-I reaction.

A recent study (*21*) demonstrated that *S. oneidensis* MR-1 was able to grow with Fe(III) in the smectite structure as the sole electron acceptor. The S-I reaction was a consequence of a bacterial survival and growth strategy. Iron(III) bound in clay minerals can be an important electron acceptor supporting the growth of bacteria in natural environments. Microbes and clay minerals can coexist in shales, siltstones, and sandstones under diagenetic conditions. Metal-reducing microbes have been discovered in sedimentary rocks from great depths (2700 m below the land surface) (*22*) and in various environments that are hot for microbial survival (up to 90° to 100°C) (*23*). These conditions are similar to those under which clay minerals undergo diagenetic reactions. Natural smectites contain structural Fe(III) to varying degrees (*24*). We suggest that microbial reduction of these quantities of Fe(III) is sufficient to reductively dissolve smectite as a trigger to the S-I reaction.

The microbially promoted S-I reaction should be considered in the study of clay mineral diagenesis. Microbial activity may be responsible for the substantial S-I reaction seen in some modern mudstones, such as those from the Nankai Trough, Japan (*25*). These young sediments have a significant percentage of illite (indicating a large extent of S-I reaction) (*25*) and sulfate-reducing microbes (*26*). It is reported that many sulfate-reducing bacteria can also reduce Fe(III) in mineral structures (*27*). Inorganic reaction is a very slow process under the site conditions.

References and Notes

1. D. R. Pevear, *Proc. Natl. Acad. Sci. U.S.A.* **96**, 3440 (1999).
2. R. L. Freed, D. R. Peacor, *Am. Assoc. Petrol. Geol. Bull.* **73**, 1223 (1989).
3. C. H. Bruce, *Am. Assoc. Petrol. Geol. Bull.* **68**, 673 (1984).
4. K. M. Brown, D. M. Saffer, B. A. Bekins, *Earth Planet. Sci. Lett.* **194**, 97 (2001).
5. R. M. Pollastro, *Clays Clay Miner.* **41**, 119 (1993).
6. C. M. Bethke, S. P. Altaner, *Clays Clay Miner.* **34**, 136 (1986).
7. H. Dong, D. R. Peacor, R. L. Freed, *Am. Mineral.* **82**, 379 (1997).
8. J. L. Keeling, M. D. Raven, W. P Gates, *Clays Clay Miner.* **48**, 537 (2000).
9. C. R. Myers, K. H. Nealson, *Science* **240**, 1319 (1988).
10. J. E. Kostka, J. W. Stucki, K. H. Nealson, J. Wu, *Clays Clay Miner.* **44**, 522 (1996).
11. H. Dong *et al.*, *Environ. Sci. Technol.* **37**, 1268 (2003).
12. E. Gaudett, J. L. Eades, R. E. Grim, *Clays Clay Miner.* **13**, 33 (1966).
13. C. E. Weaver, L. D. Pollard, Eds., *The Chemistry of Clay Minerals* (Elsevier, Amsterdam, 1973).
14. J. F. Buckley, J. C. Bevan, K. M. Brown, L. R. Johnson, V. C. Farmer, *Mineral. Mag.* **42**, 373 (1978).
15. C. M. Warshaw, thesis, The Pennsylvania State University, University Park, PA (1957).
16. D. D. Eberl, R. Nüesch, V. Sucha, S. Tsipursky, *Clays Clay Miner.* **46**, 89 (1998).
17. D. D. Eberl, V. Drits, J. Srodon, R. Nüesch, *U.S.G.S. Open-File Rep.* 96-171, 1996.
18. D. D. Eberl, V. A. Drits, J. Srodon, *Am. J. Sci.* **298**, 499 (1998).
19. E. Eslinger, P. Highsmith, D. Albers, B. DeMayo, *Clays Clay Miner.* **27**, 327 (1979).
20. J. D. Russell, B. A. Goodman, A. R. Fraser, *Clays Clay Miner.* **27**, 63 (1979).
21. J. D. Kostka, D. D. Daulton, H. Skelton, S. Dollhopf, J. W. Stucki, *Appl. Environ. Microbiol.* **68**, 6256 (2002).
22. D. R. Boone *et al.*, *Int. J. Syst. Bacteriol.* **45**, 441 (1995).
23. K. Kashefi, D. E. Holmes, A. L. Reysenbach, D. R. Lovley, *Appl. Environ. Microbiol.* **68**, 1735 (2002).
24. For example, natural smectite ranges from 0.4 mmol of Fe^{3+}/g for Wyoming Na-montmorillonite (Swy-1), to 0.5 mmol of Fe^{3+}/g for Upton montmorillonite, ~1 mmol of Fe^{3+}/g for Gulf Coast smectites, 3.5 mmol of Fe^{3+}/g for the ferruginous smectite (Swa-1), and 4.3 mmol of Fe^{3+}/g for the smectite used in this study.
25. H. Masuda, D. R. Peacor, H. Dong, *Clays Clay Miner.* **49**, 109 (2001).
26. D. W. Reed *et al.*, *Appl. Environ. Microbiol.* **68**, 3759 (2002).
27. D. R. Lovley, in *Environmental Microbe-Metal Interactions*, D. R. Lovley, Ed. (American Society for Microbiology Press, Washington, DC, 2000), pp. 3–30.

28. We thank M. D. Richardson, D. R. Peacor, and J. W. Stucki for extensive comments and discussion. This work was partially supported by the Naval Research Laboratory (contribution no. 7430-03-04). Acknowledgment is made to the donors of the Petroleum Research Fund, administered by the American Chemical Society, for support (or support in part) of this research to H.D.

Supporting Online Material

www.sciencemag.org/cgi/content/full/303/5659/830/DC1
Materials and Methods
References

3 November 2003; accepted 24 December 2003

Genome-Wide RNAi Analysis of Growth and Viability in *Drosophila* Cells

Michael Boutros,[1]*† Amy A. Kiger,[1]* Susan Armknecht,[1,2] Kim Kerr,[1,2] Marc Hild,[3] Britta Koch,[3] Stefan A. Haas,[4] Heidelberg Fly Array Consortium,[3] Renato Paro,[3] Norbert Perrimon[1,2]‡

A crucial aim upon completion of whole genome sequences is the functional analysis of all predicted genes. We have applied a high-throughput RNA-interference (RNAi) screen of 19,470 double-stranded (ds) RNAs in cultured cells to characterize the function of nearly all (91%) predicted *Drosophila* genes in cell growth and viability. We found 438 dsRNAs that identified essential genes, among which 80% lacked mutant alleles. A quantitative assay of cell number was applied to identify genes of known and uncharacterized functions. In particular, we demonstrate a role for the homolog of a mammalian acute myeloid leukemia gene (*AML1*) in cell survival. Such a systematic screen for cell phenotypes, such as cell viability, can thus be effective in characterizing functionally related genes on a genome-wide scale.

The availability of entire genome sequences stimulates the advancement of functional genomic approaches, both to accelerate the comprehensive identification of components in biological programs and to understand their functional conservation across species (*1*, *2*). In yeast and in worms, genome-wide phenotypic studies identified genes that were essential for cell fitness and development (*3*, *4*). *Drosophila* is one of the best-studied genetic organisms and is instrumental to the identification of conserved pathways with important roles from flies to humans. Treatment of cultured *Drosophila* cells with dsRNA leads to the depletion of the corresponding transcript and the generation of specific and penetrant phenotypes (*5*), providing an efficient approach for systematic loss-of-function phenotypic analyses (*6*–*9*).

Cell growth, proliferation, and survival are fundamental processes that maintain cell populations and impinge on lineage expansion and pattern formation (*10*). To identify gene functions by cell-based RNAi screens, we generated a dsRNA library targeting near-

[1]Department of Genetics, [2]Howard Hughes Medical Institute (HHMI), Harvard Medical School, Boston, MA 02115, USA. [3]Zentrum für Molekulare Biologie der Universität Heidelberg, D-69120 Heidelberg, Germany. The Heidelberg Fly Array Consortium consists of Marc Hild, Boris Beckmann, Stefan Haas, Britta Koch, Martin Vingron, Frank Sauer, Jörg Hoheisel, and Renato Paro. [4]Max-Planck Institute for Molecular Genetics, D-14195 Berlin, Germany.

*These authors contributed equally to this work.
†Present address: German Cancer Research Center, D-69120 Heidelberg, Germany.
‡To whom correspondence should be addressed. E-mail: perrimon@rascal.med.harvard.edu